Optical Interferometry for Transient Deformation Analysis

Tatiana Statsenko[†], Vasileios Chatziioannou, Wilfried Kausel

Department of Music Acoustics, University of Music and Performing Arts Vienna
[†]statsenko@mdw.ac.at

ABSTRACT

Electronic speckle pattern interferometry is performed for temporal analysis of the surface deformation of vibrating structures. This requires specially designed image processing methods in order to reconstruct the dynamic deformation of an object. The reconstruction procedure which is based on a numerical optimization algorithm is applied on a set of interferometric images recorded by a high speed camera. While designing a phase-recovery algorithm one should also consider the ill-posedness of the problem due to the ambiguity in the recorded interferometric patterns, speckle noise, and electronic noise of the camera. The presented method is applied to reconstruct temporal surface deformation of a violin body under real playing conditions. The results show the feasibility of the algorithm and the correspondence of the calculated intensity images with the experimental data.

1. INTRODUCTION

Nondestructive optical methods for inspection and analysis of surface deformations and radiated sound fields become prevalent in the musical acoustics field [1]. Various measurements of musical instruments can be performed optically, such as string motion, modal analysis, acoustic wave propagation, etc [2, 3, 4]. Most common measurement techniques involve laser Doppler vibrometry, Schlieren imaging, particle image velocimetry, holographic interferometry and electronic speckle pattern interferometry (ESPI) [1]. Each method is appropriate for performing a certain task. In case of surface deformation analysis speckle interferometry has several advantages such as full-field spatial recovery and high temporal resolution.

Temporal ESPI (TRESPI) is a general concept for speckle interferometry methods applied to record and reconstruct non-harmonic surface deformation. Initially, pulsed lasers were used for recording of transient deformations [5, 6, 7]. However, pulsed ESPI is only applied for repeatable events and thus cannot succeed in case of single transient deformation measurement because conventional cameras are not fast enough. In this case, high-speed cameras are utilized, and pulsed laser is substituted with a continuous wave laser [8, 9]. The quality of the recorded data depends directly on the camera resolution and minimum attainable exposure time.

The aim of this work is to recover out-of-plane deformation of the violin body during a single string bowing. The expected output is a dynamic deforming structure representing the relative motion of the surface in time. Section 2 describes the methodology of the measurement procedure for the TRESPI

arrangement, relevant formulas and image processing strategy. Section 3 presents the results of the deformation recovery. Section 4 discusses the issues and possible extensions of the method.

2. METHODOLOGY

Using a high-speed camera allows capturing fast deformations in the microsecond range. Small exposure time reduces the impact of the environmental noise. However, electronic noise may be an obstacle to obtain correct values of the deformation since it reinforces the intensity graininess in addition to the random speckle noise caused by the summation of the optical waves reflected by the rough surface of the object [10].

Implementation of mathematical optimization into speckle interferometry methods has shown success for the case of harmonic vibrating surfaces [11]. Instead of solving directly the inverse problem, the optimization algorithm iteratively updates vibration amplitude values to minimize the mismatch between filtered experimental data and calculated intensity. Optimization algorithm utilizes the continuousness of the surface and thus reduces the errors that may appear during pixel-by-pixel direct calculations. Applying boundary conditions and adding constraints on the possible surface profile improves the resulting quality.

2.1. Experimental setup
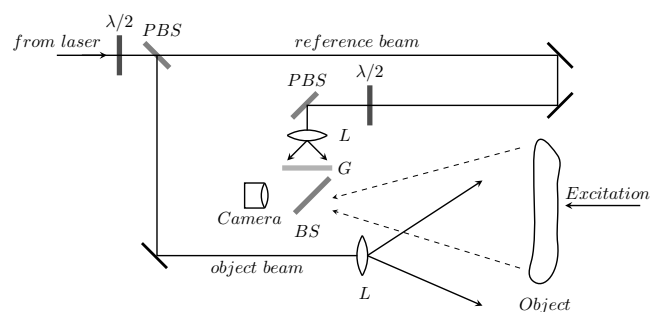
Figure 1: Experimental arrangement for a TRESPI measurement. The relative intensity of the beams and the polarization are controlled by half-wave plates ($\lambda/2$) and polarizing beam-splitters (PBS). Microscopic objective lenses (L) expand the beams. Ground glass (G) scatters the reference beam. A high-speed camera records the interference between the beam reflected from the object and the reference beam, combined by a beamsplitter (BS).

The TRESPI experimental arrangement is shown in Figure 1. The illumination is provided by a continuous wave laser (Verdi V5, Coherent Inc.) with a wavelength λ of 532 nm. The high-speed camera (Phantom v12.1, Vision Research) records interferometric frames at 21000 frames per second at a resolution of 512 by 512 pixels. The bit depth of the camera is 12 bit. Since the exposure time of the camera is extremely small (47 μs), the irradiance should be sufficient for the pixels to get enough light, so the output power of the laser is about 2 W. The violin was fixed on the optical table and excited by a bow manually. The image capturing was done using camera PCC software (Vision Research) and images were processed in MATLAB (MATLAB and Image Processing Toolbox R2014a, The MathWorks, Inc., Natick, Massachusetts, USA). The ESPI arrangements are generally sensitive to a single direction of deformation. In the current setup, the out-of-plane deformation is measured, where the plane of the object is parallel to the plane of the camera sensor.

Subtraction of the frames taken at different times produces the correlation frames which reflect the deformation profile in the form of bright and dark fringes. These fringes may be seen as lines of equal displacement of $\lambda/2$. Thereby, the qualitative assessment of the deformation that happened between two time moments during bowing is performed by the subtraction of the pair of corresponding frames. Figure 2 shows such a subtraction intensity of the violin deformation. The shape of the violin is complicated for automated analysis because the processing algorithm cannot distinguish parts such as bridge and strings. Therefore, only part of the violin is considered (256 by 256 pixels). The square region of interest that covers the quarter of the image is highlighted in Figure 2. The subtraction intensity frame shows that the tailpiece is moving differently from the violin body, which creates discontinuity of the interference pattern.

Figure 2: Qualitative ESPI image of the violin. Subtraction intensity of the interference patterns corresponding to a time difference of 4.8 ms (100 frames). The green box features the region of interest.

2.2. Theory

The intensity value recorded from the interference of two coherent beams for every pixel of the camera at time t is described as:

$$I(t) = A + B \cdot \cos(\phi(t)), \qquad (1)$$

where A is the sum of the intensities of both beams, B is the square root of their multiplication, referred to as contrast, ϕ is a global phase. The global phase is constituted of the random speckle phase and the phase offset between the two beams that changes due to the surface motion.

The coefficients A and B can be considered constant during the short image acquisition time and detected for every pixel as:

$$A = \left(\frac{\max(I(t)) + \min(I(t))}{2} \right), \qquad (2)$$

$$B = \left(\frac{\max(I(t)) - \min(I(t))}{2} \right). \qquad (3)$$

The coefficient B is the pixel modulation that shows the range of the intensity difference. If the value of B is smaller than the temporal noise, the pixel is regarded invalid since the intensity deviation is lower than noise, so it has to be removed from further processing. Therefore, a measure of pixel quality Q is introduced:

$$Q = B/N, \qquad (4)$$

where N is the noise value which is calculated as the standard deviation of the temporal intensity spatially averaged over the background region, taken from a corner of the image. Pixel quality matrix is shown in Figure 3a. Based on the Q values it is possible to automatically extract background pixels, non-moving parts and badly illuminated regions. The tailpiece part was defined and subtracted manually. The output mask of relevant pixels is shown in Figure 3b, calculated with a signal-to-noise ratio of 3 as a threshold for pixel validity.

(a) Pixel quality matrix   (b) Mask
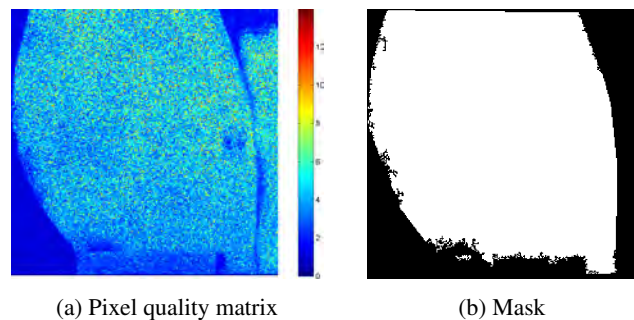
Figure 3: (a) Matrix coefficient Q and (b) mask applied to preserve valid pixels during processing.

After the intensity normalization (during which coefficients A and B are removed), the intensity at a discrete time moment t_n can be written as:

$$I(t_n) = \cos(\phi(t_n)) = \cos(\phi(t_{n-1}) + \Delta\phi(t_{n-1}, t_n)), \quad (5)$$

where $\Delta\phi(t_{n-1}, t_n)$ is the phase difference that occurs during the motion of the surface between time moments t_{n-1} and t_n. The relative deformation $\Delta D(t_{n-1}, t_n)$ linearly depends on $\Delta\phi(t_{n-1}, t_n)$ and λ:

$$\Delta D(t_{n-1}, t_n) = \frac{\lambda\Delta\phi(t_{n-1}, t_n)}{4\pi}. \quad (6)$$

The direct solution of Eq. 5 by applying an arccos function may suffer from the periodicity of the cosine function and sign ambiguity. General phase extracting methods produce a phase map with so-called "wrapped phase" that is further processed on a pixel basis in order to "unwrap" it. The algorithm based on the Rosenbrock optimization is applied to outperform pixel phase unwrapping methods. The method minimizes the target objective function while adjusting the surface displacement which is generated by bilinear interpolation on the grid points. The density of the grid points is gradually adapted to the scale of the deformation during the optimization.

The target error function F is the pixel sum of the mismatch between the normalized intensity and the intensity calculated from the predicted deformation $\Delta D(t_{n-1}, t_n)$ for every pixel with coordinates x, y:

$$F = \sum_{x,y} \left(I(t_n) - cos\left(\phi(t_{n-1}) + \frac{4\pi\Delta D(t_{n-1}, t_n)}{\lambda} \right) \right)^2. \quad (7)$$

First, the starting frame is assigned and the initial phase is calculated. Initially, the deformation is assumed positive, so that the initial phase $\phi^+(t_1)$ is calculated as:

$$\phi^+(t_1) = \arccos(I(t_1)) \cdot sign(I(t_2) - I(t_1)). \quad (8)$$

Then, the relative deformation is calculated with the respect to the first frame and $\phi^+(t_1)$. The initial guess for the deformation is a flat surface with 4 operating grid points at the edges of the image. During the optimization the surface deforms and the number of grid points increases, until the target error function is minimized or maximum value of iteration steps is attained. The optimization results in the absolute value of the deformation $|\Delta\phi(t_1, t_2)|$. The sign can be corrected through the detection of the nodal lines and differentiation between the regions that move in-phase and out-of-phase to provide the mechanical stability of the system, as proposed in [11]. After the sign correction procedure, the real phase value of $\phi(t_1)$ is obtained through pixel-by-pixel multiplication of $\phi^+(t_1)$ by the sign of the resulting phase difference:

$$\phi(t_1) = \phi^+(t_1) \cdot \text{sign}(\Delta\phi(t_1, t_2)). \quad (9)$$

This three-step algorithm that involves calculation of ϕ^+, optimization of $\Delta\phi$ and the sign correction for $\Delta\phi$ can be applied to find a phase difference between any pair of frames when the deformation does not exceed $\lambda/2$ which corresponds to 2π phase difference. However, direct summation of the obtained phase differences to obtain temporal deformation of the frame series results in a high cumulative error because of the noisy random speckle phase and the camera noise. To reduce the error, for every next recovery step $\Delta D(t_n, t_{n+1})$

the initial phase $\phi(t_n)$ is presented as the sum of the phase and the recovered deformation calculated in the previous step:

$$\phi(t_n) = \phi(t_{n-1}) + \Delta D(t_{n-1}, t_n). \quad (10)$$

The total deformation D between the first and the n-th frame is:

$$D(t_n) = \Delta D(t_1, t_2) + \Delta D(t_2, t_3) + ... + \Delta D(t_{n-1}, t_n). \quad (11)$$

3. RESULTS

During the experiment, the third string of the violin was bowed. The deformation recovery results, for various time moments for the chosen region of interest, are shown in Figure 4. Calculated intensity profiles are in good correspondence with the experimentally obtained subtraction frames. However, the effects of the cumulative error are present at the edges of the mask. This happens because the fixed boundary condition has not been applied due to the complicated shape of the mask and free boundary conditions on the top edge of the region of interest should remain. The results show the feasibility of the method in case of positive and negative deformation values, as well as in case of deformation differences higher than $\lambda/2$.

Experiment   Calculation   Deformation

(a) 0.52 ms

Experiment   Calculation   Deformation

(b) 1.1 ms

Experiment   Calculation   Deformation

(c) 2.9 ms
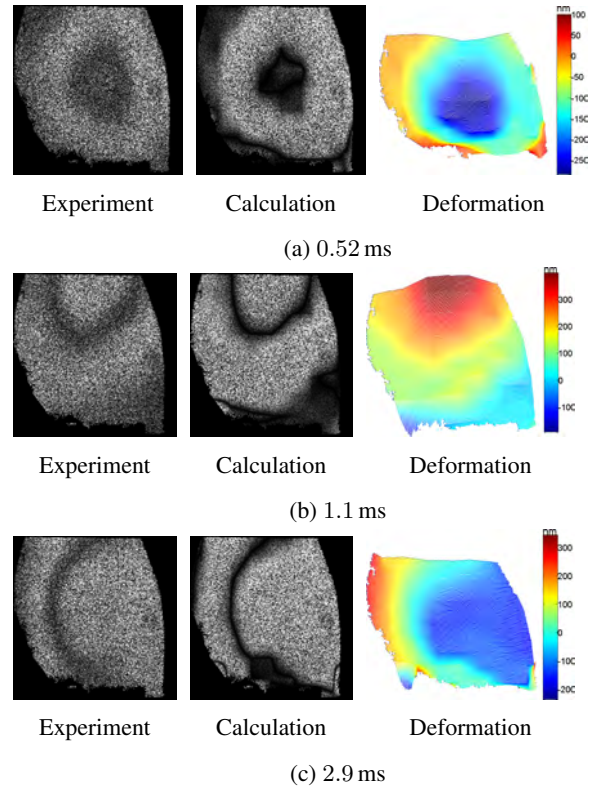
Figure 4: Results of the relative deformation reconstruction for different time intervals.

Figure 5a shows the experimentally obtained normalized intensity profile and the calculated intensity profile for a single pixel taken from the central part of the region of interest. Both contours are heavily affected by noise. However, the calculated

intensity follows the experimental data to a certain extend. This comparison proves the continuity of the deformation and robustness of the method for time range of $10\,\text{ms}$. Figure 5b shows a single pixel deformation profile taken from the central part of the region of interest.

(a) Temporal intensity

(b) Temporal deformation
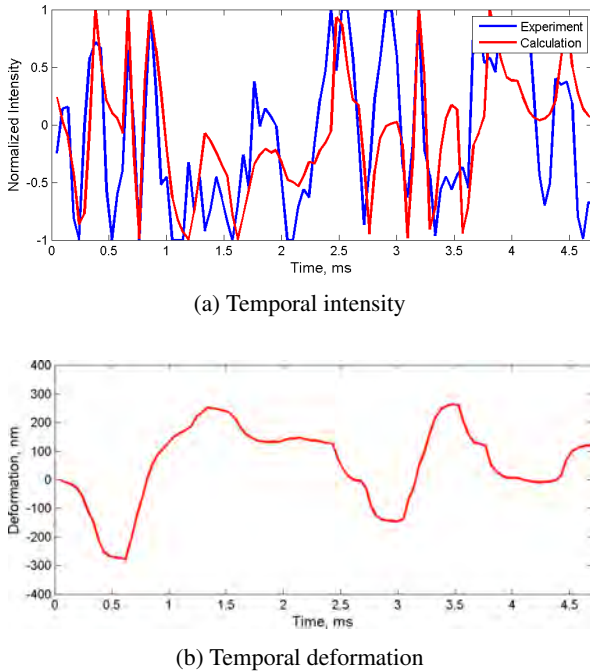
Figure 5: (a) Normalized intensity and calculated intensity of a single pixel taken from the central region of the image and (b) recovered temporal deformation.

4. CONCLUSIONS

Transient deformations of the violin body during bowing have been investigated by means of high-speed electronic speckle pattern interferometry. The presented image processing algorithm produces a dynamic out-of-plane deformation profile with high spatial and temporal resolution. This optical method can be applied in musical acoustics for transient deformation analysis of surfaces and is valuable for studying non-linear vibrations of musical instruments.

Future work will involve stability analysis, application of boundary conditions for complicated object shapes and reduction of the phase cumulative error.

5. ACKNOWLEDGMENTS

REFERENCES

[1] N. E. Molin and L. Zipser, "Optical methods of today for visualizing sound fields in musical acoustics," *Acta Acustica united with Acustica*, vol. 90, no. 4, pp. 618–628, 2004.

[2] T. R. Moore and S. A. Zietlow, "Interferometric studies of a piano soundboard," *The Journal of the Acoustical Society of America*, vol. 119, no. 3, pp. 1783–1793, 2006.

[3] G. Bissinger and D. Oliver, "3-D laser vibrometry on legendary old Italian violins," *Sound And Vibration*, vol. 41, no. 7, pp. 10–14, 2007.

[4] D. Russell, D. E. Parker, and R. S. Hughes, "Analysis of standing sound waves using holographic interferometry," *American Journal of Physics*, vol. 77, no. 8, pp. 678–682, 2009.

[5] A. Fernández, A. J. Moore, C. Pérez-López, A. F. Doval, and J. Blanco-García, "Study of transient deformations with pulsed TV holography: application to crack detection," *Applied Optics*, vol. 36, no. 10, pp. 2058–2065, 1997.

[6] C. Zang, G. Chen, D. Ewins, and I. A. Sever, "Review of current status of full-field measurement equipment hardware and software, test planning and integration tools, suggestions for future development," Tech. Rep., 2005.

[7] A. R. Ganesan, "Holographic and laser speckle methods in non-destructive testing," in *Proceedings of the National Seminar & Exhibition on Non-Destructive Evaluation*, 2009, pp. 126–130.

[8] A. J. Moore, D. P. Hand, J. S. Barton, and J. D. Jones, "Transient deformation measurement with electronic speckle pattern interferometry and a high-speed camera." *Applied Optics*, vol. 38, no. 7, pp. 1159–1162, 1999.

[9] C. Pérez-López, M. H. De la Torre-Ibarra, and F. Mendoza Santoyo, "Very high speed cw digital holographic interferometry," *Optics Express*, vol. 14, no. 21, pp. 9709–9715, 2006.

[10] M. Servin, J. C. Estrada, J. A. Quiroga, J. F. Mosiño, and M. Cywiak, "Noise in phase shifting interferometry," *Optics Express*, vol. 17, no. 11, pp. 8789–8794, 2009.

[11] T. Statsenko, V. Chatziioannou, T. Moore, and W. Kausel, "Deformation reconstruction by means of surface optimization. Part I: Time-averaged electronic speckle pattern interferometry," *Appl. Opt.*, vol. 56, no. 3, pp. 654–661, 2017.